

Microwave electrometry with Rydberg atoms in a vapor cell using microwave amplitude modulation

Jian-Hai Hao(郝建海), Feng-Dong Jia(贾凤东), Yue Cui(崔越), Yu-Han Wang(王昱寒), Fei Zhou(周飞), Xiu-Bin Liu(刘修彬), Jian Zhang(张剑), Feng Xie(谢锋), Jin-Hai Bai(白金海), Jian-Qi You(尤建琦), Yu Wang(王宇), and Zhi-Ping Zhong(钟志萍)

Citation: Chin. Phys. B, 2024, 33 (**5**): 050702. DOI: 10.1088/1674-1056/ad1a8f
Journal homepage: http://cpb.iphy.ac.cn; http://iopscience.iop.org/cpb

What follows is a list of articles you may be interested in

Loading uniform Ag_3PO_4 nanoparticles on three-dimensional peony-like WO_3 for good stability and excellent selectivity towards NH_3 at room temperature

Xingyan Shao(邵星炎), Fuchao Jia(贾福超), Tingting Liu(刘婷婷), Jiancheng Liu(刘健诚), Xiaomei Wang(王小梅), Guangchao Yin(尹广超), Na Lv(吕娜), Tong Zhou(周通), Ramachandran Rajan, and Bo Liu(刘波)
Chin. Phys. B, 2023, 32 (**8**): 080703. DOI: 10.1088/1674-1056/ac98a0

Current sensor based on diamond nitrogen-vacancy color center

Zi-Yang Shi(史子阳), Wei Gao(高伟), Qi Wang(王启), Hao Guo(郭浩), Jun Tang(唐军), Zhong-Hao Li(李中豪), Huan-Fei Wen(温焕飞), Zong-Min Ma(马宗敏), and Jun Liu(刘俊)
Chin. Phys. B, 2023, 32 (**7**): 070704. DOI: 10.1088/1674-1056/acc3fe

Construction of multi-walled carbon nanotubes/$ZnSnO_3$ heterostructures for enhanced acetone sensing performance

Liyong Du(杜丽勇) and Heming Sun(孙鹤鸣)
Chin. Phys. B, 2023, 32 (**5**): 050701. DOI: 10.1088/1674-1056/ac89da

A robust method for performance evaluation of the vapor cell for magnetometry

Zhi Liu(柳治), Sheng Zou(邹升), Kaifeng Yin(尹凯峰), Tao Shi(石韬),Junjian Tang(唐钧剑), and Heng Yuan(袁珩)
Chin. Phys. B, 2023, 32 (**4**): 040703. DOI: 10.1088/1674-1056/aca6d5

An all-optical phase detector by amplitude modulation of the local field in a Rydberg atom-based mixer

Xiu-Bin Liu(刘修彬), Feng-Dong Jia(贾凤东), Huai-Yu Zhang(张怀宇), Jiong Mei(梅炅), Wei-Chen Liang(梁玮宸), Fei Zhou(周飞), Yong-Hong Yu(俞永宏), Ya Liu(刘娅), Jian Zhang(张剑), Feng Xie(谢锋), and Zhi-Ping Zhong(钟志萍)
Chin. Phys. B, 2022, 31 (**9**): 090703. DOI: 10.1088/1674-1056/ac6dbb

---

INSTRUMENTATION AND MEASUREMENT

Microwave electrometry with Rydberg atoms in a vapor cell using microwave amplitude modulation

Jian-Hai Hao(郝建海)[1], Feng-Dong Jia(贾凤东)[1,†], Yue Cui(崔越)[1], Yu-Han Wang(王昱寒)[1], Fei Zhou(周飞)[1], Xiu-Bin Liu(刘修彬)[1], Jian Zhang(张剑)[2], Feng Xie(谢锋)[2], Jin-Hai Bai(白金海)[3,‡], Jian-Qi You(尤建琦)[3], Yu Wang(王宇)[3], and Zhi-Ping Zhong(钟志萍)[1,4]

[1] *School of Physical Sciences, University of Chinese Academy of Sciences, Beijing* 100049, *China*

[2] *Institute of Nuclear and New Energy Technology, Collaborative Innovation Center of Advanced Nuclear Energy Technology, Key Laboratory of Advanced Reactor Engineering and Safety of Ministry of Education, Tsinghua University, Beijing* 100084, *China*

[3] *Science and Technology on Metrology and Calibration Laboratory, Changcheng Institute of Metrology & Measurement, Aviation Industry Corporation of China, Beijing* 100095, *China*

[4] *CAS Center for Excellence in Topological Quantum Computation, University of Chinese Academy of Sciences, Beijing* 100190, *China*

(Received 31 October 2023; revised manuscript received 29 December 2023; accepted manuscript online 4 January 2024)

We have theoretically and experimentally studied the dispersive signal of the Rydberg atomic electromagnetically-induced transparency (EIT) Autler–Townes (AT) splitting spectra obtained using amplitude modulation of the microwave (MW) electric field. In addition to the two zero-crossing points interval $\Delta f_{\rm zeros}$, the dispersion signal has two positive maxima with an interval defined as the shoulder interval $\Delta f_{\rm sho}$, which is theoretically expected to be used to measure a much weaker MW electric field. The relationship of the MW field strength $E_{\rm MW}$ and $\Delta f_{\rm sho}$ is experimentally studied at the MW frequencies of 31.6 GHz and 9.2 GHz respectively. The results show that $\Delta f_{\rm sho}$ can be used to characterize the much weaker $E_{\rm MW}$ than that of $\Delta f_{\rm zeros}$ and the traditional EIT–AT splitting interval $\Delta f_{\rm m}$; the minimum $E_{\rm MW}$ measured by $\Delta f_{\rm sho}$ is about 30 times smaller than that by $\Delta f_{\rm m}$. As an example, the minimum $E_{\rm MW}$ at 9.2 GHz that can be characterized by $\Delta f_{\rm sho}$ is 0.056 mV/cm, which is the minimum value characterized by the frequency interval using a vapor cell without adding any auxiliary fields. The proposed method can improve the weak limit and sensitivity of $E_{\rm MW}$ measured by the spectral frequency interval, which is important in the direct measurement of weak $E_{\rm MW}$.

Keywords: quantum sensor, Rydberg atoms, electromagnetically induced transparency, amplitude modulation

PACS: 07.07.Df, 84.40.–x, 42.50.–p **DOI:** 10.1088/1674-1056/ad1a8f

1. Introduction

Quantum sensing involves utilizing quantum systems, properties, or phenomena to measure physical quantities.[1–22] Rydberg atoms, characterized by high excitation, long lifetime, and large polarizability, exhibit sensitivity to microwave (MW) frequencies, with energy level intervals falling within the microwave band. This quality makes them ideal quantum sensors for precise MW measurements. In recent years, Rydberg atom-based microwave electric field sensors have witnessed rapid development in various fields, including extreme weak field measurement,[23,24] power frequency measurement,[25] phase measurement,[26] polarization measurement,[18] and more. Through Rydberg electromagnetically-induced transparency (EIT), the introduction of MW induces the splitting of Rydberg atomic energy levels, leading to Autler–Townes (AT) splitting in EIT. Leveraging the EIT–AT effect, the MW strength can be translated into optical frequency outputs.[4] Optical frequency is well known for its absolute and direct measurability. Consequently, the measurement of microwave electric fields based on the optical frequency interval is considered the most accurate. Currently, the traditional EIT–AT splitting method achieves a minimum resolution of ∼5 mV/cm in room temperature atomic vapor cells.[4] The measurement of electric field strength using EIT–AT splitting is traceable and widely utilized for weak MW electric field calibration.[4] Consequently, the expansion of the lower limit for measuring weak MW fields through EIT–AT splitting holds significant importance.

Several methods have been developed to push the lower limit of EIT–AT splitting measurement for MW electric fields. These include the cold atom method,[27,28] MW frequency detuning,[29] auxiliary MW field,[30,31] three-photon excitation[32] and amplitude modulation (AM) dispersion.[33] Laser-cooled cold atoms, with their lower temperatures and reduced dephasing rates, significantly narrow the Rydberg EIT linewidth, enhancing precision. Kai-Yu Liao *et al*. achieved a minimum MW field resolution of 100 μV/cm using cold Rydberg atom samples,[27] while Fei Zhou *et al*. reached a 222 μV/cm limit.[28,34] However, the laser cooling of atoms requires complex equipment and has a long preparation cycle. These characteristics make the experimental platform based

†Corresponding author. E-mail: fdjia@ucas.ac.cn

‡Corresponding author. E-mail: baijh003@avic.com

© 2024 Chinese Physical Society and IOP Publishing Ltd

on cold atoms unfavorable to the subsequent development and maintenance. In addition, the atomic vapor cell has the following advantages: atomic samples are easy to obtain, the optical path is simple and easy to integrate. Therefore, Rydberg microwave electric field sensors based on vapor cells remain a vibrant research area. We outline the efforts to expand EIT–AT measurements of weak microwave fields based on atomic vapor cells. Simons *et al*. shifted the MW frequency from resonance to detuning, improving sensitivity by approximately 2 times.[29] Feng-Dong Jia *et al*. extended the lower limit by adding an auxiliary MW field, achieving two orders of magnitude lower electric field strength.[30] Jin-peng Yuan *et al*. enhanced sensitivity by two orders of magnitude using an auxiliary field at the signal MW frequency.[31] Mingzhi Han *et al*.'s bichromatic EIT in Rydberg atoms improved the minimum detectable MW electric field strength by about 3 times.[35] Fabian Ripka *et al.* achieved a 500 kHz EIT linewidth in cesium atomic vapor cells with collinear three-photon excitation, advancing the EIT–AT split linear region's lower limit by one order of magnitude.[32] Nikunjkumar Prajapati *et al*. compared two-photon and three-photon excitation, noting that narrow line features do not directly correspond to the best sensitivity.[37] Meyer *et al.* explored AM in microwave communication, and elucidated the characteristic of zero crossings and the maximum values of the dispersive curve AM MW.[36] Xiu-bin Liu *et al*. demonstrated that the spectral interval between two zero-crossing points near the EIT resonance of the dispersion signal could be utilized to measure the strength of a weak microwave electric field.[33] The method of AM MW dispersion, with its strong operability, can be applied to both two-photon and three-photon excitation, expanding the measuring range of the EIT–AT splitting region.[33]

This work represents a further exploration of the AM MW dispersion methodologies presented by Meyer *et al.*[36] and Xiubin Liu *et al.*[33] who aim to directly measure weak MW fields. In addition to exploring the zero-crossing point interval of the dispersion error signal as reported by Xiubin Liu *et al.*,[33] the work discusses the measurement of the MW electric field by the interval between the two maximum values of the dispersion error signal. The paper is structured as follows: Section 2 provides the detailed theoretical process of AM MW, Section 3 introduces the experimental system and method, Section 4 focuses on the experimental results obtained at MW frequencies of 31.6 GHz and 9.2 GHz, and Section 5 concludes the paper.

2. Theoretical model

The four levels model of ^{87}Rb atoms driven by an amplitude-modulated microwave is shown in Fig. 1. The probe laser couples the ground state $|1\rangle$ to the excited state $|2\rangle$, and the coupling laser further couples the excited state $|2\rangle$ to the Rydberg state $|3\rangle$. The ground state $|1\rangle$, excited state $|2\rangle$ and Rydberg state $|3\rangle$ form a typical ladder-type EIT configuration. To obtain the Rydberg EIT spectrum, we make the detuning of the coupling laser $\Delta_c = 0$ and the detuning of the probe laser continually Δ_p scanning between the upper and lower dashed lines of the excited state $|2\rangle$. A MW field couples the two adjacent Rydberg energy states $|3\rangle$ and $|4\rangle$. When the resonant MW field is strong enough, the EIT peak splits symmetrically into two peaks — so-called EIT–AT splitting.

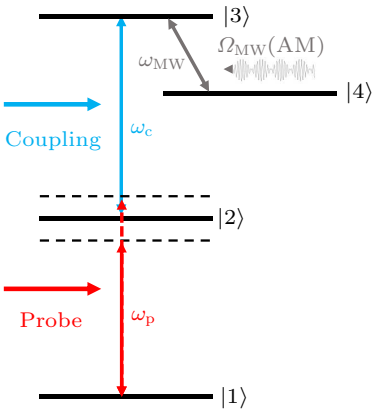


Fig. 1. Energy four-level diagram for MW amplitude modulation. The diagram involves four energy levels, two laser fields, and one amplitude-modulated MW field. Among them, the red arrow indicates the probe laser, ω_p is the angular frequency of the probe laser and it scans near the transition of $|1\rangle$ to $|2\rangle$; the blue arrow indicates the coupling laser, ω_c is the angular frequency of the coupling laser and it is always constant; the gray arrow tables the MW field, Ω_{MW}(AM) is the amplitude-modulated MW Rabi frequency.

By measuring the interval Δf_m of EIT–AT splitting, the MW electric field strength E_{MW}, which is proportional to Δf_m, can be obtained by[38]

$$E_{MW} = 2\pi \frac{\hbar}{\mu} D \Delta f_m, \tag{1}$$

where μ is the resonance transition dipole moment of the corresponding Rydberg energy levels, $\hbar$ is Planck's constant, λ_p and λ_c are the wavelengths of the probe laser and the coupling laser, respectively. D is the Doppler mismatch factor, which explains the Doppler mismatch of the reverse transmitted to the probe and coupling lasers. $D = 1$ means scanning the frequency of the coupling laser without considering Doppler mismatch.[2] In this paper, $D = \lambda_p/\lambda_c$ represents scanning the frequency of the probe laser.[2] When Δf_m is smaller than the EIT linewidth Γ_{EIT}, Δf_m cannot be obtained directly,[39] i.e., the weak MW cannot be detected by Δf_m. In order to further directly measure the weaker MW, the amplitude modulation of MW is further studied in this work.

An AM MW is performed as shown in Fig. 1, which will cause the Rydberg energy levels of $|3\rangle$ and $|4\rangle$ to be periodically shifted at the modulation frequency. It is equivalent to the frequency modulation of the EIT–AT splitting spectrum, and further dispersion signals can be obtained. We have modeled and calculated the four-level EIT–AT splitting spectra through the ATOMIC DENSITY MATRIX package.[40,41]

The weak probe condition is adopted in the modeling process, and the Doppler convolution is further obtained by numerical integration.[34,39] The detailed calculation steps of the AM EIT–AT splitting spectra are as follows:

(i) Firstly, we derive the analytical solution for ρ_{12} by solving the steady-state Lindblad equations

$$\dot{\rho} = \frac{\partial \rho}{\partial t} = -\frac{\mathrm{i}}{\hbar}[H,\rho] + \mathcal{L}, \tag{2}$$

where $\mathcal{L}$ is the Lindblad operator that represents the relaxation term related to the atomic decay process. Under the steady-state condition of $\dot{\rho}$, the analytical solution of the density matrix element ρ_{12} can be obtained from Eq. (2). Then the analytical solution for ρ_{12} is a function of the probe light detuning Δ_p, the coupling light detuning Δ_c, the microwave detuning Δ_MW, the probe light Rabi frequency Ω_p, the coupling light Rabi frequency Ω_c, and the microwave Rabi frequency Ω_MW. Subsequently, we incorporate the Doppler effect induced by gas temperature through numerical integration of the velocity distribution of atoms to get the ρ_{12_D}, as demonstrated in Ref. [39].

(ii) To obtain the EIT (or EIT–AT) splitting spectrum with probe light detuning Δ_p, one only needs to set the calculation range and step size of the probe light detuning and fix the other parameters to obtain ρ_{12_D}, from which the EIT (or EIT–AT) splitting spectrum can be derived by the magnetization χ of the medium in the cell obtained by $\chi = \left(\frac{2\mathcal{N}_0\varepsilon_{12}}{E_\mathrm{p}\varepsilon_0}\right)\rho_{12_\mathrm{D}}$. Let α be $2\pi\mathrm{Im}[\chi]/\lambda_\mathrm{p}$. Here, $\mathcal{N}_0$ is the ^{87}Rb atomic density in the cell, ε_{12} is the transition dipole moment from the ground state $|1\rangle$ to the excited state $|2\rangle$, E_p is the electric field amplitude of the probe laser, ε_0 is the vacuum permittivity, λ_p is the wavelength of the probe laser, and α is the Beer absorption coefficient of the probe laser transmitted in the medium. According to Beer–Lambert law, the transmission ratio of the probe laser before and after passing through the cell filled with ^{87}Rb atomic vapor is obtained as $T = I/I_0 = \exp(-\alpha l)$, where I_0 and I represent the optical signals before and after the probe laser passes through the cell respectively, and l represents the length of the cell containing ^{87}Rb atoms.

(iii) When solving the EIT–AT splitting spectrum for MW amplitude modulation, we introduce the MW Rabi frequency $\Omega_\mathrm{MW}(\mathrm{AM})$ at various probe light detunings Δ_p. In other words, it is equivalent to calculating the transmittance of the probe light at each probe light detuning Δ_p for different AM microwave Rabi frequencies $\Omega_\mathrm{MW}(\mathrm{AM})$. As long as the probe light detuning scanning is sufficiently slow, each probe light detuning yields results in a steady state which ensures the reliability of the calculations. By continuously varying the probe light detuning, we can obtain the spectra under microwave amplitude modulation.

(iv) Based on step (iii), the dispersion signal corresponding to the EIT–AT splitting spectrum under AM MW is obtained using modulation and demodulation codes. After modulating and demodulating the transmission signal $T\left(\Delta_\mathrm{p}, \Omega_\mathrm{MW}(\mathrm{AM})\right)$ of the probe light and performing low-pass filtering, the dispersion signal associated with the probe laser spectrum is obtained.

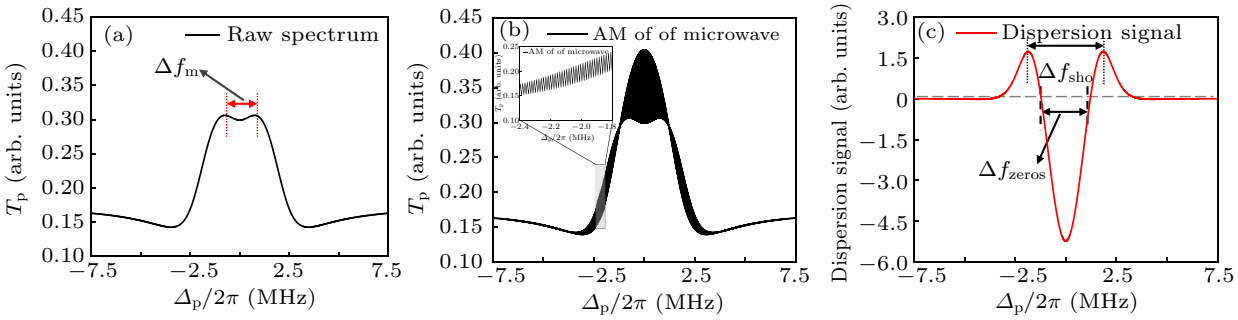


Fig. 2. Calculations of the spectrum of each stage in the AM of MW process. (a) Original EIT–AT splitting spectrum. (b) EIT–AT splitting spectrum after modulating the MW amplitude, and the modulation depth is 100%. (c) Dispersion signal after demodulation and low-pass filtering. The calculation parameters are $\Omega_\mathrm{p} = 2\pi \times 1.0$ MHz, $\Omega_\mathrm{c} = 2\pi \times 4.0$ MHz and $\Omega_\mathrm{MW} = 2\pi \times 2.5$ MHz.

We first discuss the effect of the modulation–demodulation process theoretically on the EIT–AT spectrum, as shown in Fig. 2. Figure 2(a) shows the original EIT–AT spectral signal when $\Omega_\mathrm{p} = 2\pi \times 1.0$ MHz, $\Omega_\mathrm{c} = 2\pi \times 4.0$ MHz and $\Omega_\mathrm{MW} = 2\pi \times 2.5$ MHz. Figure 2(b) shows the EIT–AT signal modulated by Ω_MW, where MD = 100%. Note that MD is the ratio of the difference between the original MW amplitude and the minimum MW amplitude after modulation to the original MW amplitude. In Fig. 2(b), the illustration depicts the spectrum details under an AM microwave electric field intensity in step (iii). Figure 2(c) shows the dispersion signal after demodulation and low-pass filtering of the modulated signal. The EIT–AT splitting interval Δf_m is $2\pi\times$ 1.51 MHz as shown in Fig. 2(a), the interval Δf_zeros between the two zero-crossing points of the dispersion signal is $2\pi\times$ 2.42 MHz as shown in Fig. 2(c), and the shoulder interval of the dispersion signal Δf_sho is $2\pi\times$ 3.71 MHz as shown in Fig. 2(c). The spectral peak resolution of the dispersion signal is significantly higher than that of the original EIT–AT spectral signal, simultaneously obtaining larger frequency intervals under the

same $\Omega_{\rm MW}$. This indicates that the lower resolution limit of $E_{\rm MW}$ can be further extended by measuring $\Delta f_{\rm sho}$.

We further investigate the effects of MD on the dispersion signal, as well as $\Delta f_{\rm zeros}$ and $\Delta f_{\rm sho}$. The dispersion signals with different MD are calculated and are shown in Fig. 3. The $\Omega_{\rm MW} = 2\pi \times 2.0$ MHz is set low enough that the traditional EIT–AT splitting $\Delta f_{\rm m}$ cannot be distinguished, as shown in the inset of Fig. 3. The corresponding dispersion signals have two zero-crossing points and a splitting symmetric double-peak. The results demonstrate that distinct dispersion signals can be acquired across a broad range of MD, thus confirming the method's universality. As the MD increases from 10% to 100%, the splitting symmetric double-peak becomes higher and clearer. $\Delta f_{\rm sho}$ as well as $\Delta f_{\rm zeros}$ becomes smaller as the MD increases due to the equivalent MW Rabi frequency becoming smaller. The relationships of $\Delta f_{\rm zeros}/\Omega_{\rm MW}$, $\Delta f_{\rm sho}/\Omega_{\rm MW}$ with MD are shown in Fig. 4. When the MD of $\Omega_{\rm MW}$ is below 60%, $\Delta f_{\rm zeros}/\Omega_{\rm MW}$, $\Delta f_{\rm sho}/\Omega_{\rm MW}$ show a good linear relationship with the MD, and as the MD becomes larger, $\Delta f_{\rm zeros}/\Omega_{\rm MW}$ and $\Delta f_{\rm sho}/\Omega_{\rm MW}$ becomes smaller. This is due to the fact that the MD of $\Omega_{\rm MW}$ becomes larger, leading to a decrease in the effective MW Rabi frequency, and $\Delta f_{\rm zeros}/\Omega_{\rm MW}$ and $\Delta f_{\rm sho}/\Omega_{\rm MW}$ also indirectly becomes smaller. When the MD of $\Omega_{\rm MW}$ is greater than 60%, the MW effective Rabi frequency constantly approaches the EIT linewidth without MW (the EIT spectral line width in the lower left corner of Fig. 4 is about $2\pi\times$ 4 MHz), then $\Delta f_{\rm zeros}/\Omega_{\rm MW}$ and $\Delta f_{\rm sho}/\Omega_{\rm MW}$ are nonlinearly related to the MD. The results confirm that $\Delta f_{\rm zeros}$ and $\Delta f_{\rm sho}$ can be clearly obtained over a large range of MD, and $\Delta f_{\rm zeros}/\Omega_{\rm MW}$, $\Delta f_{\rm sho}/\Omega_{\rm MW}$ are constant when the modulation depth is fixed.

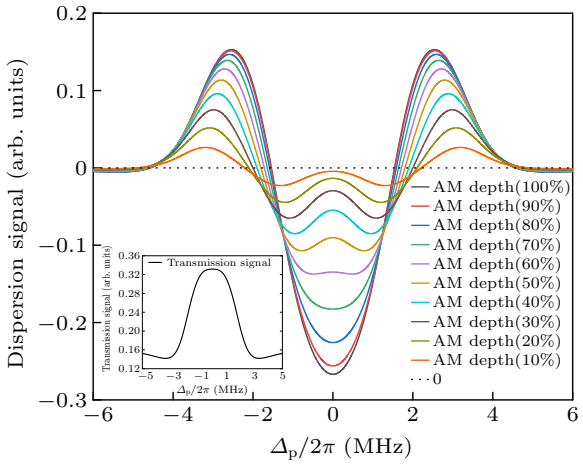


Fig. 3. Calculations of the dispersion signals with different modulation depths. The inset shows the original spectrum with $\Omega_{\rm MW} = 2\pi \times 2.0$ MHz. Note that the EIT–AT cannot be distinguished. The calculation parameters are $\Omega_{\rm p} = 2\pi \times 1.0$ MHz, $\Omega_{\rm c} = 2\pi \times 4.0$ MHz and $\Omega_{\rm MW} = 2\pi \times 2.0$ MHz.

We calculate the dispersion signal of EIT–AT at different $\Omega_{\rm MW}$ to discuss the feasibility of $\Delta f_{\rm sho}$ to measure weak fields. Figure 5 shows the numerical simulation results of EIT–AT splitting with MW field Rabi frequencies $\Omega_{\rm MW}$ from $2\pi \times 0.7$ MHz to $2\pi \times 3$ MHz where figure 5(a) represents the EIT–AT splitting spectra at $\Omega_{\rm MW}$ without amplitude modulation. $\Delta f_{\rm m}$ becomes smaller when $\Omega_{\rm MW}$ decreases, and $\Delta f_{\rm m}$ becomes indistinguishable when $\Omega_{\rm MW}$ is less than $2\pi \times 2.2$ MHz. Figure 5(b) represents the dispersion error signal after an amplitude modulation of $\Omega_{\rm MW}$. When $\Omega_{\rm MW}$ is much smaller than $2\pi \times 2.2$ MHz, $\Delta f_{\rm sho}$ can still be observed.

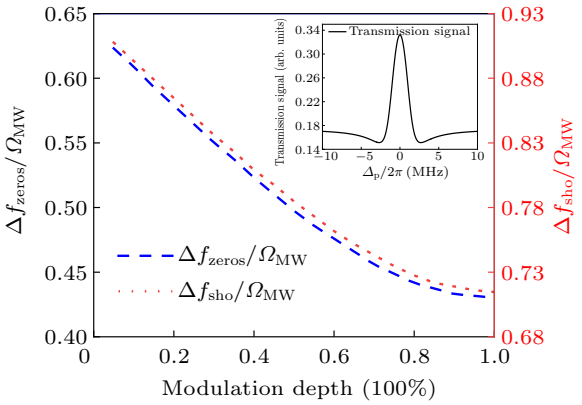


Fig. 4. Calculation results of the relationship between the interval of the zero crossing of dispersion signals $\Delta f_{\rm zeros}$, the dispersion signal shoulder interval $\Delta f_{\rm sho}$ and different modulation depths. The blue dashed line represents $\Delta f_{\rm zeros}/\Omega_{\rm MW}$; the red dotted line represents $\Delta f_{\rm sho}/\Omega_{\rm MW}$. The calculation parameters are $\Omega_{\rm p} = 2\pi \times 1.0$ MHz, $\Omega_{\rm c} = 2\pi \times 4.0$ MHz, $\Omega_{\rm MW} = 2\pi \times 7.0$ MHz, and the amplitude modulation depth of $\Omega_{\rm MW}$ is 5%–100%. The inset shows that the EIT spectrum with $\Omega_{\rm MW} = 0$ and the line width of the EIT is about $2\pi \times 4$ MHz.

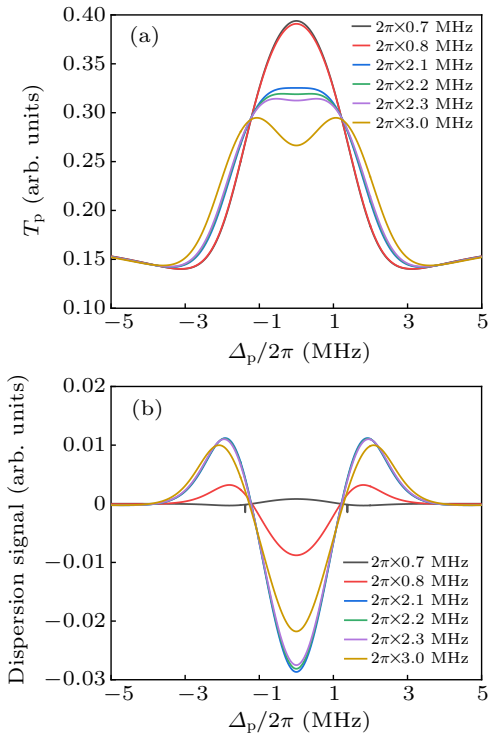


Fig. 5. Numerical simulation results of EIT–AT splitting spectra at MW field Rabi frequencies $\Omega_{\rm MW}$ between $2\pi \times 0.7$ MHz and $2\pi \times 3$ MHz. (a) EIT–AT spectra without modulation. (b) Corresponding dispersion error signal with modulation depth MD = 100%.

The relationship between $\Delta f_{\rm m}$, $\Delta f_{\rm zeros}$ and $\Delta f_{\rm sho}$ for $\Omega_{\rm MW}$

between $2\pi \times 0.7$ MHz and $2\pi \times 10$ MHz is shown in Fig. 6. As shown in the black solid line in Fig. 6, $\Delta f_{\rm m}$ decreases linearly as $\Omega_{\rm MW}$ decreases, but when $\Omega_{\rm MW}$ is less than $2\pi \times 3.4$ MHz, the linear characteristic of $\Delta f_{\rm m}$ disappears and finally becomes indistinguishable with $\Omega_{\rm MW} = 2\pi \times 2.0$ MHz. The blue dashed line in Fig. 6, $\Delta f_{\rm zeros}$ decreases monotonically with $\Omega_{\rm MW}$ decreasing, and $\Delta f_{\rm zeros}$ becomes unchanging when $\Omega_{\rm MW} < 1.5$ MHz. The red dotted line in Fig. 6, $\Delta f_{\rm sho}$ decreases monotonically as $\Omega_{\rm MW}$ decreases, and $\Delta f_{\rm sho}$ becomes unchanging when $\Omega_{\rm MW}$ is $2\pi \times 0.8$ MHz. The results show that $\Delta f_{\rm sho}$ has a significant resolution advantage over $\Delta f_{\rm m}$ and $\Delta f_{\rm zeros}$ when measuring weak MW fields.

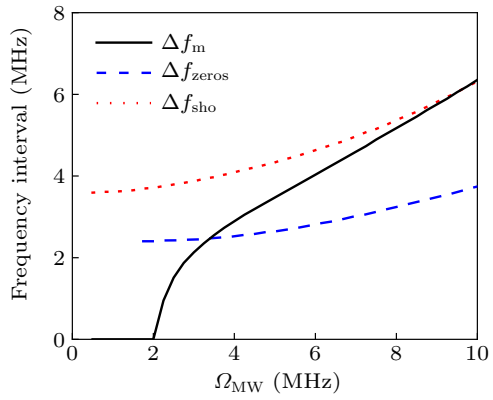


Fig. 6. Calculation results with $\Delta f_{\rm m}$, $\Delta f_{\rm zeros}$ and $\Delta f_{\rm sho}$ with respect to $\Omega_{\rm MW}$. The solid black line represents the original EIT–AT splitting interval $\Delta f_{\rm m}$; the blue dashed line represents the interval of the zero crossing of dispersion signals $\Delta f_{\rm zeros}$; the red dotted line represents the dispersion signal shoulder interval $\Delta f_{\rm sho}$. The calculation parameters are $\Omega_{\rm MW} = 2\pi \times 0.7$ MHz–$2\pi \times 10$ MHz, $\Omega_{\rm p} = 2\pi \times 1.0$ MHz, $\Omega_{\rm c} = 2\pi \times 4.0$ MHz, and the modulation depth is 100%.

3. Experimental system and methods

We have experimentally verified the above proposal in a rubidium vapor cell at room temperature. The schematic diagram of the experimental system is shown in Fig. 7. The diameter and length of the Rb vapor cell at room temperature were 25 mm and 75 mm, respectively. In the four energy levels proposed in Fig. 1, when the MW field frequency to be measured is 31.6 GHz by ^{87}Rb atoms, the four energy levels $|1\rangle$, $|2\rangle$, $|3\rangle$, and $|4\rangle$ in the theoretical model can be selected as $5S_{1/2}$, $5P_{3/2}$, $41D_{5/2}$, and $42P_{3/2}$, respectively, as shown in Fig. 8, where the probe laser ($\lambda_{\rm p} \sim 780$ nm, DL100, Toptica) is generated by a tunable diode laser whose frequency is locked at the transition of ^{87}Rb $5S_{1/2} \rightarrow 5P_{3/2}$. The coupling light ($\lambda_{\rm c} \sim 480$ nm, TA-SHG Pro, Toptica) is generated by a frequency doubling diode laser, and its frequency is locked at the resonant transition of ^{87}Rb $5P_{3/2} \rightarrow 41D_{5/2}$ by the Zeeman modulation EIT method.[42] The probe and coupling lasers overlap and transmit in reverse on the central axis of the Rb cell. The MW amplitude modulation is realized by inputting a TTL or sin signal into the amplitude modulation port of the microwave source, and finally the modulated MW is irradiated on the vapor cell through a microwave antenna (LB-28-15-C-KF). A photodetector (PDA36A2, Thorlabs) is used to receive the transmission signal of the probe laser through the ^{87}Rb vapor cell and is then recorded by an oscilloscope.

The MW field in the experiment was provided by an MW source (Keysight Technologies, E8257D) and radiated by a horn antenna of the corresponding frequency (see below for specific models) to the Rb vapor cell. In the experiments, we generated a modulation signal consisting of a high level of 0 V and a low level of −0.999 V, utilizing a 10 kHz sinusoidal amplitude modulation signal from a signal source (RIGOL, DG4202). This signal was connected to the Ext 1 input port of the microwave source (Keysight Technologies, E8257D); here 0 V corresponds to the output power set by the microwave source, while −0.999 V effectively deactivated the microwave source's output, achieving an RF output with a modulation depth of 100% and a modulation frequency of 10 kHz. In fact, an MD of 0–100% can be achieved by changing the value of the low level from 0 to −0.999 V. Our experiment shows that we only needed to attenuate the microwave power, and there was no need to double it. This approach is more practical for real-world applications, for example, attenuate and modulate the MW amplitude by adding a TTL switch to the microwave cable connected to the horn.

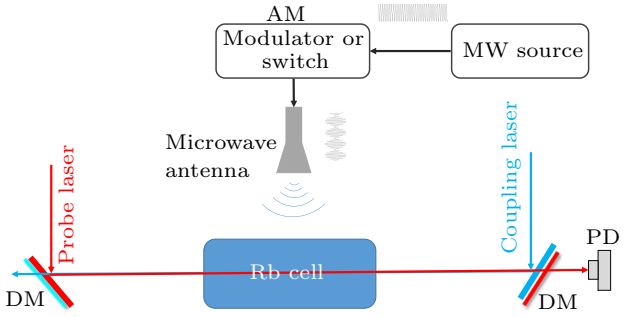


Fig. 7. The experimental setup for measuring the MW strength by the amplitude modulation method. The red and blue lines with arrows represent the probe laser and coupling laser, respectively. A modulator or switch is used to modulate MW amplitude. DM is the dichroic mirror, and PD is the photodetector.

In the experiments, MW fields at two different frequencies (9.2 GHz and 31.6 GHz, respectively) are measured in this work. Specifically, the microwave horns employed in the experiment were 9.2 GHz (A-INFO, LB-90-15-C-SF) and 31.6 GHz (A-INFO, LB-28-15-C-KF). Note that the horn was placed 550 mm away from the Rb cell during the experiment, ensuring compliance with the far-field conditions. The schematic diagram of the energy level is shown in Fig. 8. For the MW field at 31.6 GHz, the coupling laser coupling energy level is $5P_{3/2} \rightarrow 41D_{5/2}$ and the MW field coupling energy level is $41D_{5/2} \rightarrow 42P_{3/2}$, corresponding to a resonant transition dipole moment of $955\,a_0 e$ calculated by Ref. [43], where a_0 is the Bohr radius and e is the elementary charge. For the

MW field with 9.2 GHz, the coupling laser coupling energy level is $5P_{3/2} \rightarrow 61D_{5/2}$ and MW field coupling energy level is $61D_{5/2} \rightarrow 62P_{3/2}$, corresponding to a resonant transition dipole moment of $2160a_0e$ calculated by Ref. [43]. The MW field, probe laser, and coupling laser are all linearly polarized. A sin signal is used to modulate the MW source as discussed above. The range of modulation frequency in this work can be set from 1 to 99 kHz, and the MD of the MW can be changed from 0% to 100%. The Rydberg EIT–AT spectra are obtained by scanning the probe laser frequency near the EIT resonance using an acousto-optic modulator (AOM). The modulated EIT signal is sent to a lock-in amplifier (LI5640, NF Corporation) for demodulation, and then the dispersion signal can be obtained.

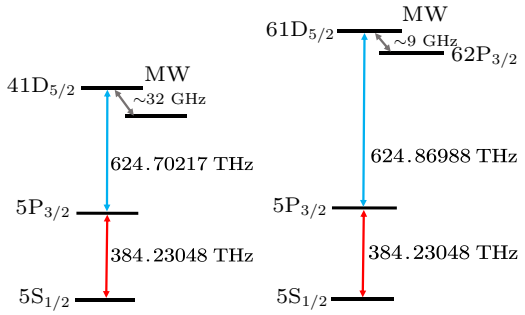


Fig. 8. Selection of energy levels of rubidium for measuring MW with a frequency of 31.6 GHz and 9.2 GHz, respectively. In order to clearly show the energy levels, the energy level positions are not drawn strictly at real intervals.

4. Results and discussion

We first studied the Rydberg EIT–AT spectrum obtained without modulation of the MW and the dispersion signal obtained by modulation. The experimental results are shown in Fig. 9. Figure 9(a) shows the original EIT–AT splitting spectrum where the signal-to-noise ratio (SNR) is relatively poor. The experimental data clearly exhibits a periodic noise. It was determined that this noise signal originated from other equipment within the laboratory, most likely stemming from a nearby switch power supply. In fact, this noise signal can be effectively eliminated through modulating coupling light intensity (as depicted in Fig. 9(b)), or by modulating the amplitude of the microwave field (as shown in Fig. 9(c)). The solid black line in Fig. 9(b) indicates the EIT–AT spectrum obtained by modulating the coupling laser amplitude, the red dashed line indicates the signal demodulated by the lock-in amplifier, and the SNR of the demodulated spectrum is improved by 17.5 dB compared with the original EIT–AT spectrum in Fig. 9(a). The solid black line in Fig. 9(c) represents the EIT–AT spectrum obtained by modulating the MW amplitude, and the red dashed line represents the dispersion signal obtained by MW amplitude modulation. The SNR of the dispersion signal is improved by 20.2 dB compared with the original EIT–AT spectrum in Fig. 9(a). It can be seen that the dispersion signal has two zero-crossing points whose interval is defined as Δf_{zeros}. Xiu-bin Liu *et al*. have demonstrated that Δf_{zeros} extends the lower limit of MW measurement by a factor of 6 compared to the conventional EIT–AT splitting method.[33] More interestingly, there are two positive maxima of the dispersive signal whose interval is defined as Δf_{sho}; Δf_{sho} is larger than Δf_{zeros} which could reflect the weaker E_{MW}. Compared with the former and based on the theoretical model in Section 2, the lower limit of the MW electric field that can be measured by this method can be also lower.

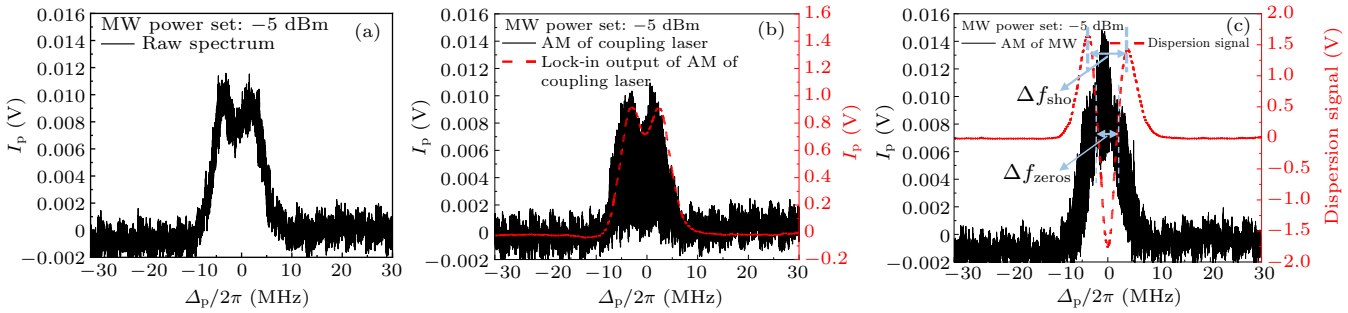


Fig. 9. Experimental examples of the spectra: (a) original EIT–AT splitting spectrum without AM modulation, (b) the coupling laser amplitude modulation spectrum, and (c) the MW amplitude modulation spectrum, respectively. The amplitude modulation frequency is 10 kHz and the amplitude modulation depth is 100%.

A smaller modulation depth can lead to larger splitting, however, the amplitude and signal-to-noise ratio of the dispersion signal itself are also greatly reduced. In fact, we have conducted theoretical and experimental research with modulation depths ranging from 10% to 100%. In our experiments, we were able to obtain a sufficiently clear dispersion signal at a modulation depth of 10%, allowing for the clear determination of shoulder intervals and zero-crossing intervals. These results demonstrate that the SNR of spectral reading signals can be improved within the modulation depth range of 10% to 100%, leading to the acquisition of clear dispersion signals. This validates the universality of our method. At a modulation depth of 100% for microwave amplitude modulation, we observed a more pronounced peak in the dispersion signal's shoulder, further enhancing the distinguishing ability of the shoulder interval at weak microwave strength. Additionally, achieving

100% amplitude modulation was simpler in real applications, such as by adding a TTL switch to the microwave antenna cable. Consequently, our experimental focus was primarily on utilizing a 100% modulation depth for in-depth research.

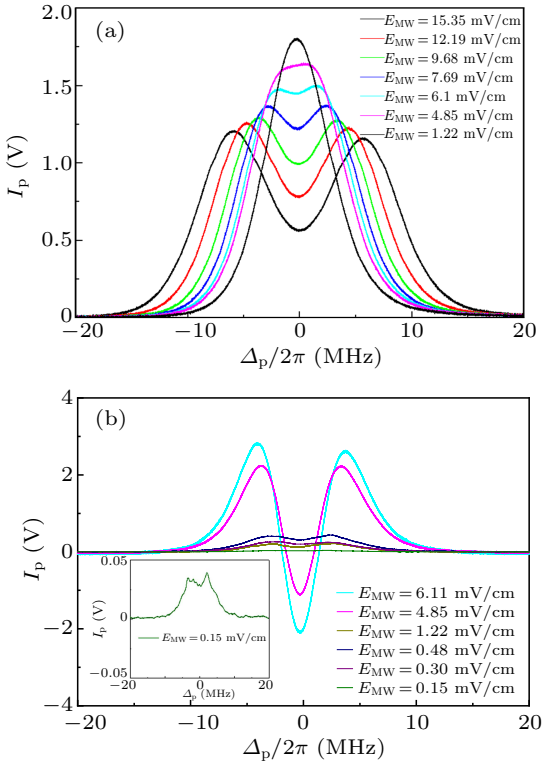


Fig. 10. Experimental conventional Rydberg EIT–AT splitting spectra and the dispersion signal obtained by AM modulation of MW. (a) EIT–AT splitting spectra with the E_{MW} reduced from 15.351 mV/cm to 1.219 mV/cm. (b) Dispersion signal with the E_{MW} reduced from 6.115 mV/cm to 0.155 mV/cm. The inset shows that the dispersion signal with $E_{MW} = 0.155$ mV/cm. In the experiment, the modulation frequency of MW is 10 kHz and the modulation depth is 100%.

We then performed a detailed analysis of the spectra obtained by the conventional method[4] and the AM modulation method at 31.6 GHz. For the conventional method, when the MW electric field is continuously varied between 1.219 mV/cm and 15.351 mV/cm, a series of spectral signals corresponding to the EIT–AT splitting are obtained, as shown in Fig. 10(a). The experimental results show that Δf_m becomes indistinguishable as E_{MW} gradually decreases to 4.854 mV/cm. Even for $E_{MW} = 4.854$ mV/cm, we cannot read Δf_m directly from the graph, but can only get it indirectly by spectrum analysis. The reason is that E_{MW} is too small; the two dressed-level intervals by MW are smaller than the EIT linewidth Γ_{EIT} which results in the fact that the Rydberg EIT–AT splitting cannot be directly observed. Furthermore, when E_{MW} is smaller than 1.219 mV/cm, Δf_m cannot be obtained even by spectrum analysis. In contrast, as shown in Fig. 10(b), when the E_{MW} is smaller than 1.219 mV/cm, the two maxima in the dispersive signal can still be distinguished and easily obtained f_{sho}. We find that Δf_{sho} are still present under the weak field where the EIT–AT splitting is indistinguishable, which confirms that Δf_{sho} can be used to measure and characterize the weak MW electric field strength. More interestingly, Δf_{sho} is still clearly distinguished when the interval Δf_{zeros} does not exist with the much weaker MW field, as shown in Fig. 10(b).

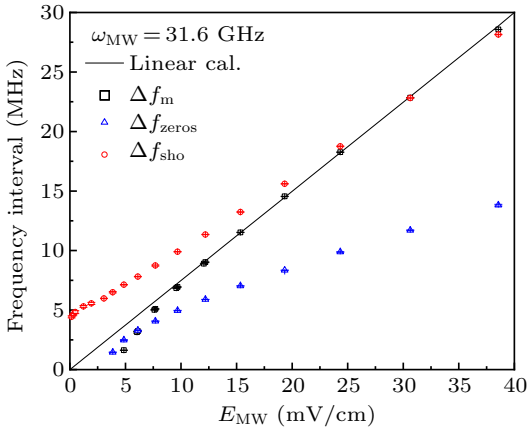


Fig. 11. Experimental results of Δf_m, Δf_{zeros} and Δf_{sho} versus E_{MW} at MW frequency of 31.6 GHz. The black hollow squares represent the results of the traditional EIT–AT splitting method by Δf_m. The blue hollow triangles represent the experimental results of the interval of zero crossing of the dispersion signals method by Δf_{zeros}. The red hollow circles represent the experimental results of the dispersion signal shoulder interval method by Δf_{sho}. The modulation frequency of MW is 10 kHz and the modulation depth is 100%.

Next, we discuss in detail the experimental results of the Δf_m method, Δf_{zeros} method, and Δf_{sho} method at an MW frequency of 31.6 GHz. The Δf_m, Δf_{zeros} and Δf_{sho} corresponding to different E_{MW} can be further obtained from Fig. 10, and the results are shown in Fig. 11. The black hollow square dots indicate the variation of the EIT–AT splitting interval Δf_m with the MW field E_{MW} by the conventional EIT–AT splitting method, which exhibits a linear feature when $E_{MW} > 7.694$ mV/cm. As E_{MW} decreases, the Δf_m becomes smaller than the linear prediction by Eq. (1) and cannot be observed when $E_{MW} < 4.854$ mV/cm. For Δf_{zeros} method as shown as the blue hollow triangles in Fig. 11, Δf_{zeros} cannot be observed with $E_{MW} < 3.856$ mV/cm in this work. Note that the improvement by Δf_{zeros} is not as good as the results of Xiu-bin Liu *et al.*[33] This is because the experimental parameters in our experiment were optimized to obtain clearer Δf_{sho} resolution instead of Δf_{zeros}. More especially, to achieve the optimal Δf_{zeros} in Ref. [33], a modulation depth of 10% is chosen, aiming to obtain a broader Δf_{zeros} interval, as a small modulation depth may not yield a clear dispersion signal, which becomes particularly problematic at extremely low microwave strength. Consequently, in this study, we opted for a modulation depth of 100%. While this sacrifices the resolution of Δf_{zeros} intervals, it enhances the SNR of the dispersion signals in weak fields. Experiments have demonstrated that, even when Δf_{zeros} is not present, Δf_{sho} remains discernible, indicating an improved ability to detect weak fields. As a result, for the Δf_{sho} method as shown as the red hollow circles in Fig. 11, Δf_{sho} is still clearly observed even when $E_{MW} = 0.155$ mV/cm, and the

monotonic relationship between $E_{\rm MW}$ and $\Delta f_{\rm sho}$ is always retained. As the results with MW frequency of 31.6 GHz, $\Delta f_{\rm sho}$ in this work is better than $\Delta f_{\rm zeros}$ method,[33] and the lower limit of $E_{\rm MW}$ is even 32 times improved than that of conventional EIT–AT splitting $\Delta f_{\rm m}$.

We further discuss and analyze the measurement results of the three methods at 9.2 GHz MW frequency in order to verify the effectiveness of the proposed method for MW measurement at 1–40 GHz. The results are shown in Fig. 12. The process of analysis is similar to the above. The results with MW frequency of 9.2 GHz show that the lower limit of $E_{\rm MW} = 0.056$ mV/cm is even 31 times improved than that of the conventional EIT–AT splitting method.[4]

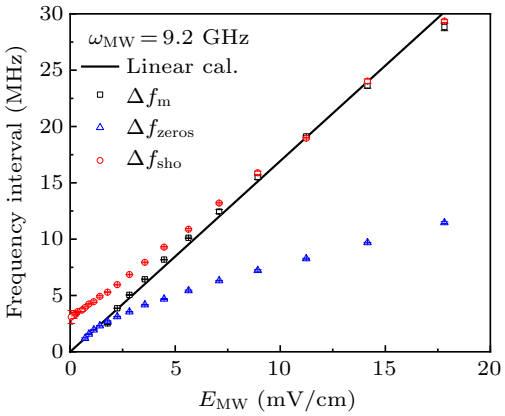


Fig. 12. Experimental results of $\Delta f_{\rm m}$, $\Delta f_{\rm zeros}$ and $\Delta f_{\rm sho}$ versus $E_{\rm MW}$ at MW frequency of 9.2 GHz. The black hollow squares represent the results of the traditional EIT–AT splitting method by $\Delta f_{\rm m}$. The blue hollow triangles represent the experimental results of the interval of zero crossing of the dispersion signals method by $\Delta f_{\rm zeros}$. The red hollow circles represent the experimental results of the dispersion signal shoulder interval method by $\Delta f_{\rm sho}$. The modulation frequency of MW is 10 kHz and the modulation depth is 100%.

Across the measurements at two different frequencies, we observe a qualitative consistency in the relationship between $\Delta f_{\rm zeros}$ ($\Delta f_{\rm sho}$) and $E_{\rm MW}$, as shown in Figs. 11 and 12. The distinct slopes can be attributed to variations in the resonant dipole moments corresponding to these frequencies. In our experimental setup, we sought to measure the field strength of weak-field microwaves using two different microwave frequencies within the same experimental system. However, due to the absence of microwave horns covering the 0–40 GHz range in our laboratory, we opted for two horns designed for use at these frequencies. Given the varying sizes of these microwave horns across the two frequency bands (with horn size decreasing as microwave frequency increases), it was challenging to ensure complete consistency in the distance between the MW horn and the cell while maintaining far-field conditions when switching between microwave horns. This discrepancy accounts for the inconsistent quality of the $\Delta f_{\rm zeros}$ and $\Delta f_{\rm sho}$ experiments in two frequencies. In our actual experiments, we employed a traditional EIT–AT splitting interval $\Delta f_{\rm m}$ to calibrate $\Delta f_{\rm zeros}$ and $\Delta f_{\rm sho}$ for each band (horn). After calibration, we were able to achieve reproducible experimental results under identical experimental conditions. The stability and repeatability of the experimental results were maintained, primarily under consistent parameters such as modulation depth and lock-in phase amplifier settings. Therefore, by utilizing the traditional EIT–AT splitting method to calibrate the electric field intensity corresponding to the dispersion shoulder interval, we are able to characterize very weak fields using the dispersion shoulder interval.

The shoulder interval of dispersion signals $\Delta f_{\rm sho}$ displays a monotonous relationship with microwave intensity that proves challenging to fully encapsulate with an analytical formula, as shown in Figs. 6, 11, and 12. This relationship remains entirely reproducible when experimental parameters are held constant. Therefore, by employing the traditional EIT–AT splitting interval $\Delta f_{\rm m}$ as a reference for calibrating the electric field intensity associated with the dispersion shoulder interval, it becomes feasible to characterize the weak field.

Finally, a comparison of the minimum MW strength $E_{\rm MW}$ measured by different methods is shown in Table 1, with MW frequencies of 31.6 GHz and 9.2 GHz respectively. $E_{\rm MW}(\Delta f_{\rm m})_{\rm min}$, $E_{\rm MW}(\Delta f_{\rm zeros})_{\rm min}$ and $E_{\rm MW}(\Delta f_{\rm sho})_{\rm min}$ are the lower limits for measuring the distinguishable MW field strength at specific MW frequencies. When the MW frequency is 9.2 GHz, the lower limit of the $E_{\rm MW}$ that can be measured is 0.056 mV/cm, which is much smaller than that when the MW frequency is 31.6 GHz. The quantum number of the two adjacent Rydberg levels is relatively high when the MW frequency is 9.2 GHz, which makes the electric dipole moment between the two Rydberg levels large. According to Eq. (1), for the same spectral splitting interval, the greater the electric dipole moment, the lower the limit of the measurable microwave field. Since then, this work has verified that the $\Delta f_{\rm sho}$ method has advantages over traditional methods and the $\Delta f_{\rm zeros}$ method in the MW field measurement under the experimental conditions of MW frequencies of 31.6 GHz and 9.2 GHz. This is also predicted in the theoretical part of Section 2.

Table 1. Comparison of the minimum MW strength $E_{\rm MW}$ measured by different methods, with MW frequencies of 31.6 GHz and 9.2 GHz respectively.

Frequency	$E_{\rm MW}(\Delta f_{\rm m})_{\rm min}$	$E_{\rm MW}(\Delta f_{\rm zeros})_{\rm min}$	$E_{\rm MW}(\Delta f_{\rm sho})_{\rm min}$
31.6 GHz	4.854 ± 0.022 mV/cm	3.856 ± 0.032 mV/cm	0.152 ± 0.055 mV/cm
9.2 GHz	1.782 ± 0.056 mV/cm	0.709 ± 0.036 mV/cm	0.056 ± 0.031 mV/cm

5. Conclusion

We have theoretically and experimentally studied the dispersion signal of the Rydberg atomic electromagnetic induction transparent Autler–Townes splitting spectrum obtained using amplitude modulation of the MW field in detail. Theoretically, we first demonstrate the process of microwave electric field amplitude modulation and demodulation to obtain the dispersion signals by numerical simulation. Compared with the traditional EIT–AT splitting interval $\Delta f_{\rm m}$, the dispersion signal provides two spectral intervals, namely, the interval of the two zero-crossing points $\Delta f_{\rm zeros}$ and the interval of two positive maxima $\Delta f_{\rm sho}$. Then we study the effect of modulation depth on the dispersion signals in detail, and the results show that distinct dispersion signals can be acquired across a broad range of modulation depths, thus confirming the method's universality. The greater the modulation depth, the more pronounced the characteristics of maxima ($\Delta f_{\rm sho}$) in the dispersion signal. When the modulation depth is fixed, the ratio of $\Delta f_{\rm zeros}/\Omega_{\rm MW}$ or $\Delta f_{\rm sho}/\Omega_{\rm MW}$ is fixed, which proves that $\Delta f_{\rm zeros}$ and $\Delta f_{\rm sho}$ can be used to characterize microwave electric field strength $E_{\rm MW}$. The traditional EIT–AT spectra and the corresponding dispersion signals at 100% modulation depth at different $\Omega_{\rm MW}$ are theoretically calculated in detail. By comparing $\Delta f_{\rm m}$, $\Delta f_{\rm zeros}$, and $\Delta f_{\rm sho}$ with $\Omega_{\rm MW}$, the results show that $\Delta f_{\rm sho}$ can characterize much weaker microwave electric fields than that of $\Delta f_{\rm m}$, $\Delta f_{\rm zeros}$. Experimentally, we have studied the relationship of MW field strength $E_{\rm MW}$ and $\Delta f_{\rm sho}$ in a rubidium vapor cell at the MW frequencies of 31.6 GHz and 9.2 GHz, respectively. The results show that the microwave electric field amplitude modulation method improves the spectral signal-to-noise ratio, and more interestingly, $\Delta f_{\rm sho}$ can be used to characterize the much weaker $E_{\rm MW}$ than $\Delta f_{\rm m}$ and $\Delta f_{\rm zeros}$, the minimum $E_{\rm MW}$ measured by $\Delta f_{\rm sho}$ is about 30 times smaller than the conventional EIT–AT splitting method. As an example, the minimum $E_{\rm MW}$ at 9.2 GHz that can be characterized by $\Delta f_{\rm sho}$ is 0.056 $\pm$0.031 mV/cm, which is the minimum value we know that can be characterized by frequency interval using a vapor cell without adding any auxiliary fields. The proposed method can reduce the weak limit of $E_{\rm MW}$ measured by the spectral frequency interval and is suited to different excitation schemes, which is important in the direct measurement of weak $E_{\rm MW}$.

Acknowledgements

Project supported by Beijing Natural Science Foundation (Grant No. 1212014), the National Key Research and Development Program of China (Grant Nos. 2017YFA0304900 and 2017YFA0402300), the National Natural Science Foundation of China (Grant Nos. 11604334, 11604177, and U2031125), the Key Research Program of the Chinese Academy of Sciences (Grant No. XDPB08-3), the Open Research Fund Program of the State Key Laboratory of Low-Dimensional Quantum Physics (Grant No. KF201807), the Fundamental Research Funds for the Central Universities, and Youth Innovation Promotion Association CAS.

References

[1] Gallagher Thomas F 1994 *Cambridge Monographs on Atomic, Molecular and Chemical Physics*
[2] Mohapatra A K, Jackson T R and Adams C S 2007 *Phys. Rev. Lett.* **98** 113003
[3] Fleischhauer M, Imamoglu A and Marangos J P 2005 *Rev. Mod. Phys.* **77** 633
[4] Sedlacek J, Schwettman A, Kübler H, Löw R, Pfau T and Shaffer J P 2012 *Nat. Phys.* **8** 819
[5] Drever R W P, Hall J L, Kowalski F V, Hough J, Ford G M, Munley A J and Ward H 1983 *Appl. Phys. B* **31** 97
[6] Hirata S, Akatsuka T, Ohtake Y and Morinaga A 2014 *Appl. Phys. Express* **7** 022705
[7] Abel R P, Mohapatra A K, Bason M G, Pritchard J D, Weatherill K J, Raitzsch U and Adams C S 2009 *Appl. Phys. Lett.* **94** 3086305
[8] Jiao Y C, Li J K, Wang L M, Zhang H, Zhang L J, Zhao J M and Jia S T 2016 *Chin. Phys. B* **25** 053201
[9] Bao S X, Zhang H, Zhou J, Zhang L J, Zhao J M, Xiao L T and Jia S T 2016 *Phys. Rev. A* **94** 043822
[10] Lin Y, Wu F C, Mao R Q, Yao J W, Liu Y, An Q and Fu Y Q 2022 *Acta Phys. Sin.* **71** 170702 (in Chinese)
[11] Mao R Q, Lin Y, Yang K, An Q and Fu Y Q 2023 *IEEE Antennas and Wireless Propagation Letters* **22** 352 Q
[12] Wu B, Lin Y, Liao D W, Liu Y, An Q and Fu Y Q 2022 *Electronics Letters* **58** 914
[13] Hu J L, Li H Q, Song R, Bai J, Jiao Y C, Zhao J M and Jia S T 2022 *Appl. Phys. Lett.* **121** 014002
[14] You S H, Cai M H, Zhang S S, Xu Z S and Liu H P 2022 *Opt. Express* **30** 16619
[15] Cai M H, Xu Z S, You S H and Liu H P 2022 *Photonics* **9** 250
[16] Feng Z G, Liu X C, Zhang Y Y, Ruan W M, Song Z F and Qu J F 2023 *Opt. Express* **31** 1692
[17] Degen C L, Reinhard F and Cappellaro P 2017 *Rev. Mod. Phys.* **89** 035002
[18] Wang Y H, Jia F D, Hao J H, Cui Y, Zhou F, Liu X B, Mei J, Yu Y H, Liu Y, Zhang J, Xie F and Zhong Z Z 2023 *Opt. Express* **31** 10449
[19] Cui Y, Jia F D, Hao J H, Wang Y H, Zhou F, Liu X B, Yu Y H, Mei J, Bai J H, Bao Y Y, Hu D, Wang Y, Liu Y, Zhang J, Xie F and Zhong Z P 2023 *Phys. Rev. A* **107** 043102
[20] Li Y, Zhang J, Wang Y, Du H, Wu J, Liu W, Mei F, Ma J, Xiao L and Jia S 2022 *Light: Science & Applications* **11** 13
[21] Wang Y, Zhang J H, Li Y, Wu J, Liu W, Mei F, Hu Y, Xiao L, Ma J, Chin C and Jia S 2022 *Phys. Rev. Lett.* **129** 103401
[22] Wang Y, Du H, Li Y, Mei F, Hu Y, Xiao L, Ma J and Jia S 2023 *Light: Science & Applications 12* 50
[23] Hao L, Xue Y, Fan J, Bai J, Jiao Y and Zhao J 2020 *Chin. Phys. B* **29** 033201
[24] Hao L, Xue Y, Fan J, Jiao Y, Zhao J and Jia S 2019 *Chin. Phys. B* **28** 053202
[25] Liu W, Zhang L and Wang T 2023 *Chin. Phys. B* **32** 053203
[26] Liu X B, Jia F D, Zhang H Y, Mei J, Liang W C, Zhou F, Yu Y H, Liu Y, Zhang J, Xie F and Zhong Z P 2022 *Chin. Phys. B* **31** 090703
[27] Liao K Y, Tu H T, Yang S Z, Chen C J, Liu X H, Liang J, Zhang X D, Yan H and Zhu S L 2020 *Phys. Rev. A* **101** 053432
[28] Zhou F, Jia F, Liu X, Yu Y, Mei J, Zhang J, Xie F and Zhong Z 2023 *J. Phys. B: Atom. Mol. Opt. Phys.* **56** 025501
[29] Simons M T, Gordon J A, Holloway C L, Anderson D A, Miller S A and Raithel G 2016 *Appl. Phys. Lett.* **108** 174101
[30] Jia F D, Liu X B, Mei J, Yu Y H, Zhang H Y, Lin Z Q, Dong H Y, Zhang J, Xie F and Zhong Z P 2021 *Phys. Rev. A* **103** 063113
[31] Yuan J, Jin T, Wang L, Xiao L and Jia S 2022 *Laser Physics Letters* **19** 125207
[32] Ripka F, Lui C, Schmidt M, Kubler H and Shaffer J P 2022 *Optical and Quantum Sensing and Precision Metrology II*

[33] Liu X, Jia F, Zhang H, Mei J, Yu Y, Liang W, Zhang J, Xie F and Zhong Z 2021 *AIP Advances* **11** 085127

[34] Zhou F, Jia F D, Liu X B, Zhang J, Xie F and Zhong Z P 2023 *Acta Phys. Sin.* **72** 045204 (in Chinese)

[35] Han M, Hao H, Song X, Yin Z, Parniak M, Jia Z and Peng Y 2023 *EPJ Quantum Technology* **10** 28

[36] Meyer D H, Cox K C, Fatemi F K and Kunz P D 2018 *Appl. Phys. Lett.* **112** 211108

[37] Prajapati N, Bhusal N, Rotunno A P, Berweger S, Simons M T, Artusio-Glimpse A B, Wang Y J, Bottomley E, Fan H and Holloway C L 2022 arXiv: 2211.11848 [physics.atom-ph].

[38] Holloway C L, Gordon J A, Jefferts S, Schwarzkopf A, Anderson D A, Miller S A, Thaicharoen N and Raithel G 2014 *IEEE Transactions on Antennas and Propagation* **62** 6169

[39] Holloway C L, Simons M T, Gordon J A, Dienstfrey A, Anderson D A and Raithel G 2017 *J. Appl. Phys.* **121** 233106

[40] Auzinsh M, Budker D and Rochester S 2010 *Optically Polarized Atoms: Understanding light-atom interactions*

[41] S.Rochester , https://www.rochesterscientific.com/.

[42] Jia F, Zhang J, Zhang L, Wang F, Mei J, Yu Y, Zhong Z and Xie F 2020 *Appl. Opt.* **59** 2108

[43] Šibalić N, Pritchard J D, Adams C S and Weatherill K J 2017 *Computer Physics Communications* **220** 319